Progress In Electromagnetics Research C, Vol. 73, 55–64, 2017

Efficient Dual-Band Asymmetric Transmission of Linearly Polarized Wave Using a Chiral Metamaterial

Yajun Liu[1, 2, 3], Song Xia[1, *], Hongyu Shi[2], Anxue Zhang[2], and Zhuo Xu[1]

Abstract—In this paper, a three-layered chiral metamaterial composed of three twisted split-ring resonators is proposed and investigated. The simulated and measured results show that the proposed metamaterial can achieve efficient asymmetric transmission of linearly polarized wave and cross-polarization conversion for two distinct bands: X (6.95–10.05 GHz) and Ku (15.55–18.47 GHz). In the X-band, an incident y-polarized wave is almost converted to a x-polarized wave, while an incident x-polarized wave is completely blocked from passing through the structure. In the Ku-band, an incident x-polarized wave is almost converted to a y-polarized wave, while an incident y-polarized wave is blocked from passing through the structure. Moreover, the simulated and measured results confirm that the proposed metamaterial has a good robustness to misalignment, which provides convenience for fabricating in practical applications. Finally, the physical mechanism of this dual-band asymmetric transmission effect can be explained based on the different resonant modes of the proposed structure.

1. INTRODUCTION

Electromagnetic (EM) metamaterials (MMs), which are artificial composites materials, have attracted considerable research attention because they have unique EM properties that do not exist in natural materials. Over the past few years, more sophisticated MMs have been proposed to achieve numerous custom functionalities, including negative refractive index [1], invisibility cloaking [2], perfect lenses [3], and linear or/to circular polarization conversion [4–6]. In 2006, an interesting EM phenomenon called asymmetric transmission (AT) was first observed for circularly polarized wave in a planar chiral MM (CMM) by Fedotov et al. [7]. This AT effect originates from the fact that a circularly polarized incident wave has different polarization conversion efficiencies for the two opposite propagation directions. In addition, it is found that the AT effect is quite distinct from the nonreciprocity of the Faraday effect, and can be described using the Lorentz Jones matrix. Since the concept of AT was proposed, many MM-based structures with AT effect for circularly polarized wave have been proposed and discussed in the literature, including split-ring resonators (SRRs) [8], twisted meander lines [9], and asymmetrically split rings (ASRs) [10]. In 2010, Menzel et al. designed a novel three-dimensional chiral optical MM that realized the AT effect for both linearly and circularly polarized waves by breaking the mirror symmetry in the direction perpendicular to the propagation direction [11]. Subsequently, various CMM structures that could be used to achieve AT for linearly polarized wave have been demonstrated [12–17]. However, in the earlier proposed CMM, the AT effect is usually in a narrow band which separates them from the practical applications. More recently, great efforts have been devoted to achieve broadband (or dual-band) as well as high efficiency AT effect for linearly polarized wave [18–23]. Shi et al. [18]

Received 16 January 2017, Accepted 27 March 2017, Scheduled 10 April 2017

* Corresponding author: Song Xia (sxia@mail.xjtu.edu.cn).

[1] Electronic Materials Research Laboratory, Key Laboratory of the Ministry of Education & International Center for Dielectric Research, Xi'an Jiaotong University, Xi'an 710049, China. [2] School of Electronic and Information Engineering, Xi'an Jiaotong University, Xi'an 710049, China. [3] College of Physics and Optoelectronic Technology, Baoji University of Arts and Sciences, Baoji 721016, China.

proposed that a bi-layered CMM consisting of double I-shaped resonators realized dual-band AT for linearly polarized wave. Based on a Fabry-Perot-like cavity, a three-layered MM has been proposed to obtain a broadband AT effect only for a specific linearly polarized wave at microwave frequencies [21]. Song et al. reported a CMM composed of three layers of metasurfaces that exhibits a multi-band AT of linearly polarized wave [22]. Studying the aforementioned designed CMM structures, one tends to have an impression that multi-layered planar CMM seems more attractive in achieving efficient and broadband (or dual-band) AT effect.

In this paper, we propose a simple three-layered CMM composed of three twisted SRRs, which achieve two bands AT and 90° polarization rotator of a linearly polarized wave. The simulated and measured results show that the CMM is nearly transparent to an incident linearly polarized wave in two distinct AT bands, where a linearly polarized incident wave can be efficiently converted to its cross-polarized wave and can be transmitted, while the same linearly polarized wave is blocked from traveling in the opposite direction. Each AT band can be switched on/off by changing the polarization state of the incident wave [18]. Moreover, the simulated and measured results confirm that the proposed structure has a good robustness to misalignment, which provides convenience for fabricating in practical applications. Finally, the physical mechanism of dual-band AT can be explained based on the different resonant modes of the proposed structure.

2. THEORETICAL ANALYSIS

To better understand the AT effect of EM wave in the proposed CMM, the T transmission matrix is used. This matrix describes the relationship between the incident and transmitted electric fields [24]:

$$\begin{pmatrix} T_x \\ T_y \end{pmatrix} = \begin{pmatrix} t_{xx} & t_{xy} \\ t_{yx} & t_{yy} \end{pmatrix} \begin{pmatrix} I_x \\ I_y \end{pmatrix} = T^f_{lin} \begin{pmatrix} I_x \\ I_y \end{pmatrix} \tag{1}$$

where the index f and lin indicate propagation in forward direction (along $-z$ direction) and linearly polarized wave incidence, respectively; t_{xx} and t_{yy} are the co-polarization transmission coefficients, and t_{xy} and t_{yx} are the cross-polarization transmission coefficients. Based on reciprocal theory, the T matrix for a linearly polarized wave propagation in backward direction (along $+z$ direction) can be expressed as [24]:

$$T^b_{lin} = \begin{pmatrix} t_{xx} & -t_{yx} \\ -t_{xy} & t_{yy} \end{pmatrix} \tag{2}$$

Using Eqs. (1) and (2), the AT for a linearly polarized wave can be characterized using the parameter Δ, which is defined as the difference between the transmitted intensities in the two opposing propagation directions ($+z$ and $-z$). Therefore, the AT parameter Δ for the x- and y-polarized wave can be defined as [11, 12]:

$$\Delta^x_{lin} = |t_{yx}|^2 - |t_{xy}|^2 = -\Delta^y_{lin} \tag{3}$$

According to Eq. (3), AT will appear for a linearly polarized wave provided that the cross-polarization transmission coefficients are different. Therefore, a large difference between two perpendicular incident wave of cross-polarization will lead to significant AT.

3. STRUCTURE DESIGN AND SIMULATION

In previous studies, a structure composed of two twisted stacked SRRs has been shown to form a chiral structure and exhibits a high-strength AT effect due to the near-field coupling between the first and second SRRs [14]. However, this structure is only applicable to a specific linear polarization. As the analysis in [22] shows, a multi-layered structure based on Fabry-Perot-like cavity can realize a multi-band AT effect. Based on these findings, we propose a simple three-layered CMM that uses three twisted SRRs to achieve efficient AT for both y-polarized and x-polarized incident waves.

Figure 1 shows the unit cell of the CMM, which is composed of three SRRs printed on the two sides of the dielectric substrate. The front and back metallic structures are composed of the same SRRs, but with split direction that are perpendicular to each other; the middle metallic layer is another SRRs, and its split direction is rotated at an angle of 45° with respect to the x axis. The dielectric substrate

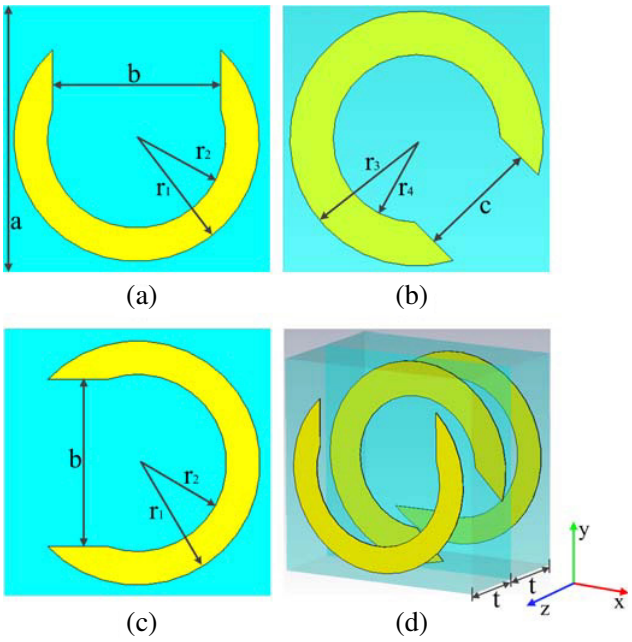

Figure 1. Schematics of the unit cell of the three-layered chiral structure. (a) Top metallic layer, (b) middle metallic layer, and (c) bottom metallic layer, (d) perspective view of the proposed unit cell.

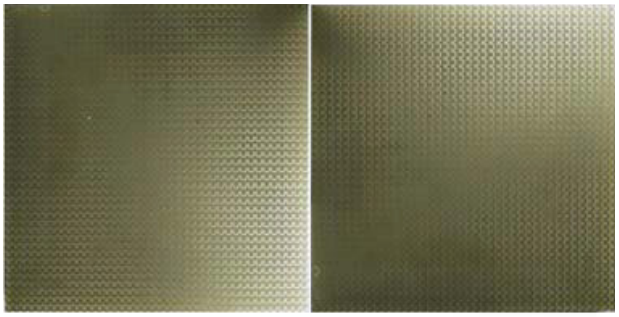

Figure 2. Photographs of the sample. (a) Top layer, and (b) bottom layer.

thickness $t = 3.0\,\text{mm}$, the dielectric constant $\varepsilon_r = 2.65$, and the loss tangent $\tan\delta = 0.0012$. The CMM unit cell periodicity is $a = 8.0\,\text{mm}$. The other geometric parameters of the structure are $b = 5.0\,\text{mm}$, $c = 3.6\,\text{mm}$, $r_1 = 3.65\,\text{mm}$, $r_2 = 2.65\,\text{mm}$, $r_3 = 3.8\,\text{mm}$, and $r_4 = 2.5\,\text{mm}$. The three metallic layers were modeled as 0.035-mm-thick copper films with electrical conductivity of $\sigma = 5.8 \times 10^7\,\text{S/m}$.

The numerical simulation was performed using the commercially available software CST Microwave Studio, which is based on the finite integration technique. In the simulation, periodic conditions are used in the x- and y-directions, and absorbing boundary conditions are used in the z-direction. The model is excited using a Floquet port with a normally linearly polarized incident wave.

For the experiment, the designed sample was fabricated in a 40×40 unit cell ($320\,\text{mm} \times 320\,\text{mm}$) structure by a conventional printed circuit board (PCB) technique using the same structural parameters as the simulation model. A photograph of the fabricated sample is shown in Fig. 2. The selected dielectric substrate material was F4B and had a thickness of 3.0 mm, a dielectric constant $\varepsilon_r = 2.65$, and a loss tangent $\tan\delta = 0.0012$. The complex transmission coefficients of the fabricated sample were carried out in an EM anechoic chamber. The rectangular waveguide standard gain horn antennas are connected to a vector analyzer (Agilent E836B) by coaxial cable to measure the transmission coefficients from 6 to 20 GHz. In the experiment, by changing the orientation of the two horn antennas, all components of the wave transmission (the complex Jones matrix) for different polarizations were measured.

4. RESULTS AND DISCUSSION

Based on the above theoretical analysis, we simulated and measured the transmission coefficients (i.e., the complex Jones matrix) in the CMM for both the forward ($-z$) and backward ($+z$) propagating waves, with results as shown in Fig. 3. The measured results show excellent agreement with the simulated ones across the entire frequency range of interest, and any small differences can be attributed to machining and measurement errors. Figs. 3(a) and (b) show the simulated and measured results for the linearly polarized wave propagation in forward direction. It can be seen that the co-polarization transmission

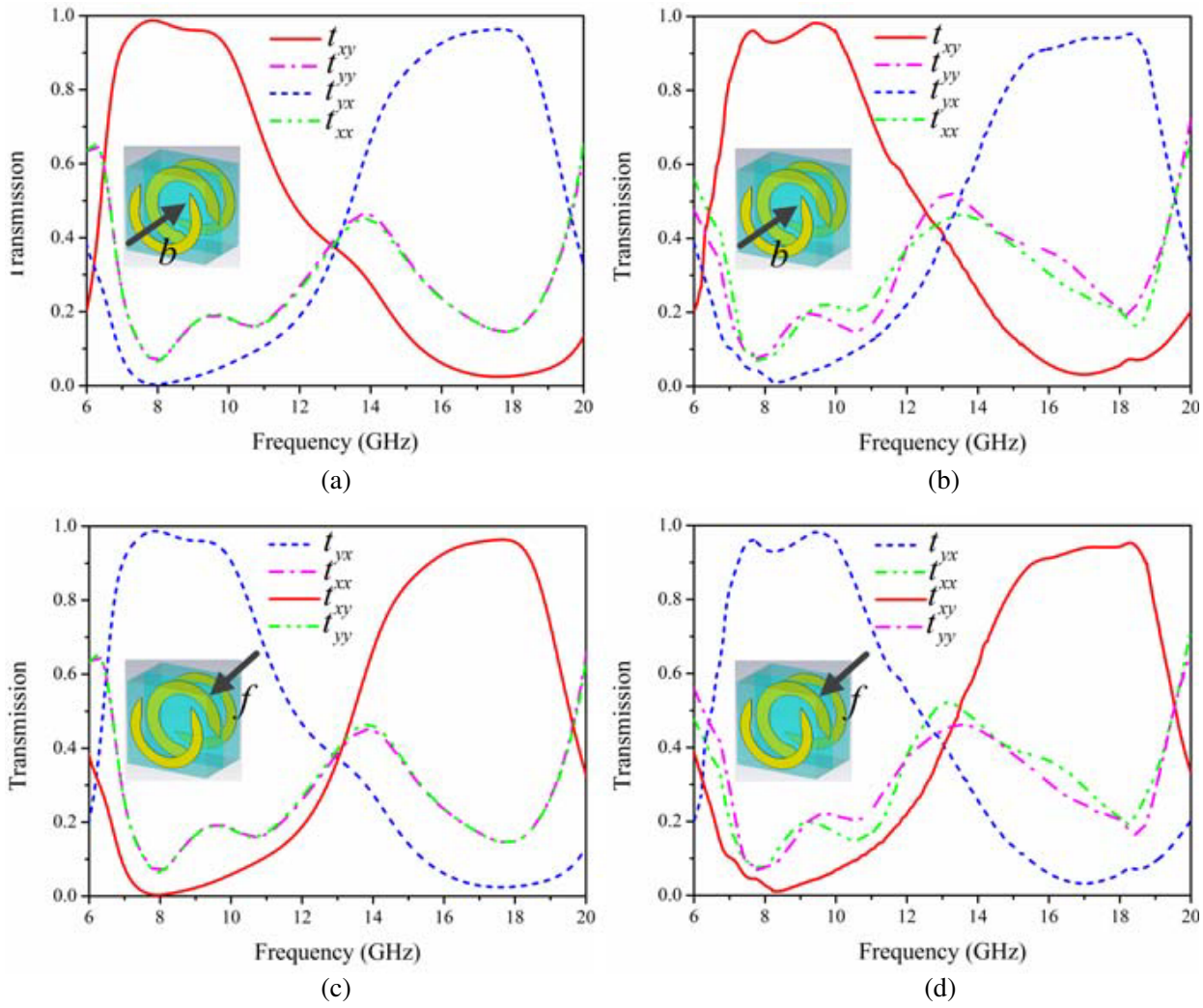

Figure 3. Simulated ((a) and (c)) and measured ((b) and (d)) transmission coefficients for forward ((a) and (b)) and backward ((c) and (d)) propagating waves.

coefficients t_{xx} for the x-polarized wave and t_{yy} for the y-polarized wave are identical over the range from 6 to 20 GHz. In contrast to co-polarization transmission coefficients, the cross-polarization transmission coefficients t_{xy} apparently differs from t_{yx} over the whole frequency range we consider. These two conditions indicate the presence of the AT effect for linearly polarized wave and the absence of the AT effect for circularly polarized wave for this chiral CMM [11]. As shown in Fig. 3(a), when the y-polarized wave propagates along the structure in forward direction, the cross-polarization transmission coefficients t_{xy} is more than 0.90 in the range from 6.95 to 10.05 GHz, and there is an obvious t_{xy} peak that can reach 0.986 at around 7.86 GHz. However, the co-polarization transmission coefficients, t_{yy} and t_{xx}, have values of less than 0.29. This means that the y-polarized incident wave is completely converted to x-polarized wave, while x-polarized incident wave cannot pass through the CMM. Additionally, when the x-polarized wave propagates along the structure in forward direction in the range from 15.55 to 18.47 GHz, the cross-polarization transmission coefficients t_{yx} is more than 0.90, and t_{yx} reaches a maximum of 0.963 at around 17.65 GHz, while the co-polarization transmission coefficients t_{xx} and t_{yy} are less than 0.30. This means that the x-polarized incident wave is almost completely converted to y-polarized wave, while y-polarized incident wave cannot pass through the CMM. These results indicate that the CMM can achieve y-to-x polarization conversion in a low frequency pass band (6.95–10.05 GHz) and can also achieve x-to-y polarization conversion in a higher frequency pass band (15.55–18.47 GHz).

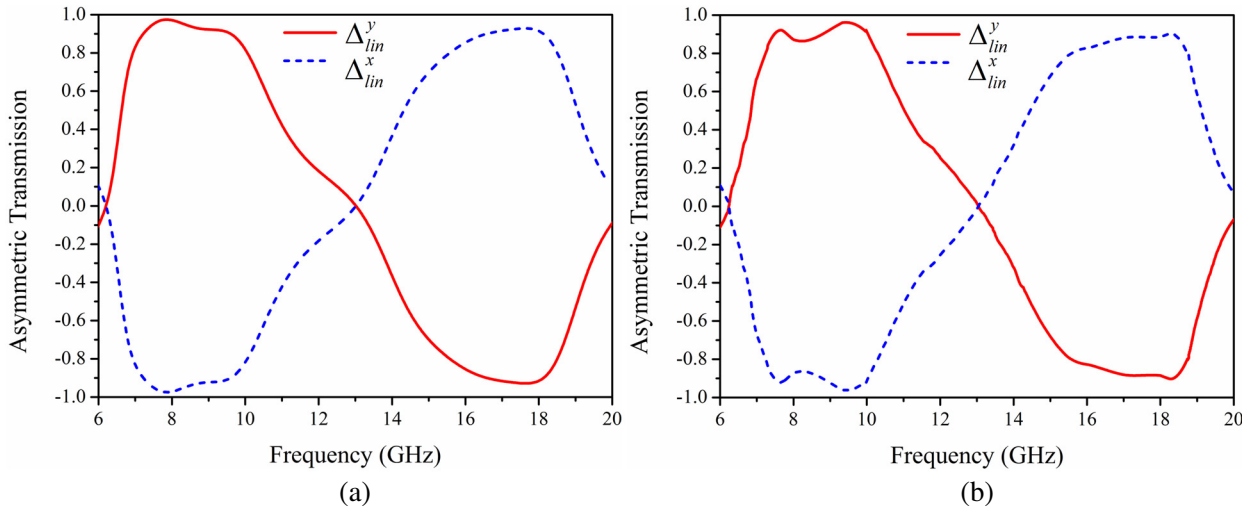

Figure 4. (a) Simulated and (b) measured asymmetric transmission parameter Δ of the linearly polarized wave.

Figs. 3(c) and (d) show the transmission coefficients for linearly polarized wave propagation in backward direction. From Figs. 3(a) and (c), when the propagation direction is reversed, t_{xy} and t_{yx} interchange with each other in the two pass bands.

Based on Eq. (3), the AT parameter Δ was calculated for a linearly polarized wave propagation in forward direction, and the result is shown in Fig. 4. From Fig. 4(a), we see that the AT parameter Δ^y_{lin} is greater than 0.8 in the range from 6.95 to 10.05 GHz, while Δ^x_{lin} is less than -0.8. This fact implies that y/x-polarized wave along forward propagation direction is mostly allowed/forbidden in the range from 6.95 to 10.05 GHz. However, the opposite result is observed in the range from 15.55 to 18.47 GHz. This is because the asymmetric parameter Δ^x_{lin} has a value of more than 0.8, while Δ^y_{lin} is less than -0.8, which means that x/y-polarized wave along forward propagation direction is mostly allowed/forbidden in the range from 15.55 to 18.47 GHz. The measured results for the AT parameter Δ are shown in Fig. 4(b). The measured results are coinciding with the simulated results and further confirm the existence of the dual-band AT effect in the proposed structure.

Given that the CMM also has a high polarization conversion capacity in conjunction with the AT effect, we also calculated the polarization azimuth rotation angle ψ and the ellipticity η of the transmitted wave for x- and y-polarized waves propagation in forward direction. The polarization azimuth rotation angle ψ and the ellipticity η of $y(x)$-polarized wave propagation in forward direction can be defined as [25, 26]:

$$\begin{aligned} \psi &= \frac{1}{2}\tan^{-1}\left\{\frac{2R\cos(\varphi)}{1-R^2}\right\} \\ \eta &= \frac{1}{2}\sin^{-1}\left\{\frac{2R\sin(\varphi)}{1+R^2}\right\} \end{aligned} \tag{4}$$

where $R = |t_{ij}|/|t_{jj}|$ and $\varphi = \arg(t_{ij}) - \arg(t_{jj})$, the index i and j in transmission coefficients t_{ij} correspond to the polarization states of the transmitted and incident waves. The polarization azimuth rotation angle ψ and ellipticity η, which were calculated based on the simulation results, are shown in Figs. 5(a) and (b). Fig. 5(a) shows that the polarization azimuth rotation angle ψ of the y-polarized incident wave almost exceeds 80° (absolute value) over the range from 7.28 to 10.05 GHz, while the ellipticity η is nearly 0° (where the absolute value of η is less than 5° from 7.28 to 10.05 GHz). This indicates that the y-polarized incident wave is converted to its cross-polarized wave in the range from 7.28 to 10.05 GHz. In contrast, as shown in Fig. 5(b), for x-polarized incident wave in the range from 16.46 to 18.47 GHz, the polarization azimuth rotation angle ψ is almost exceeds 80°, and the ellipticity η is nearly 0° (where the absolute value of η is less than 10° from 16.46 to 18.47 GHz). This indicates

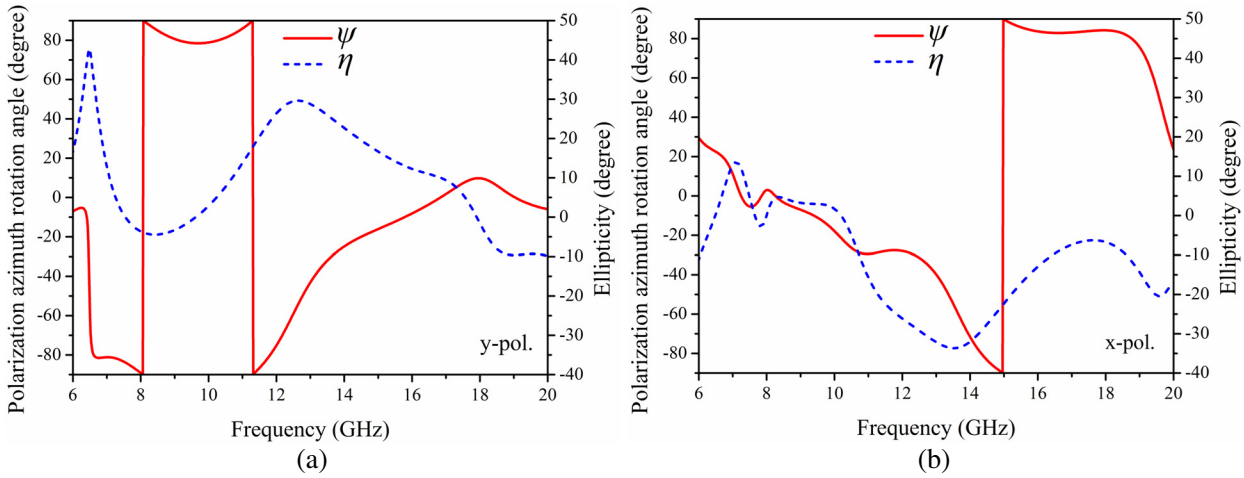

Figure 5. Simulated polarization azimuth rotation angle Ψ (red solid line) and ellipticity η (blue dashed line) for (a) y-polarized incident wave, and (b) x-polarized incident wave in forward direction.

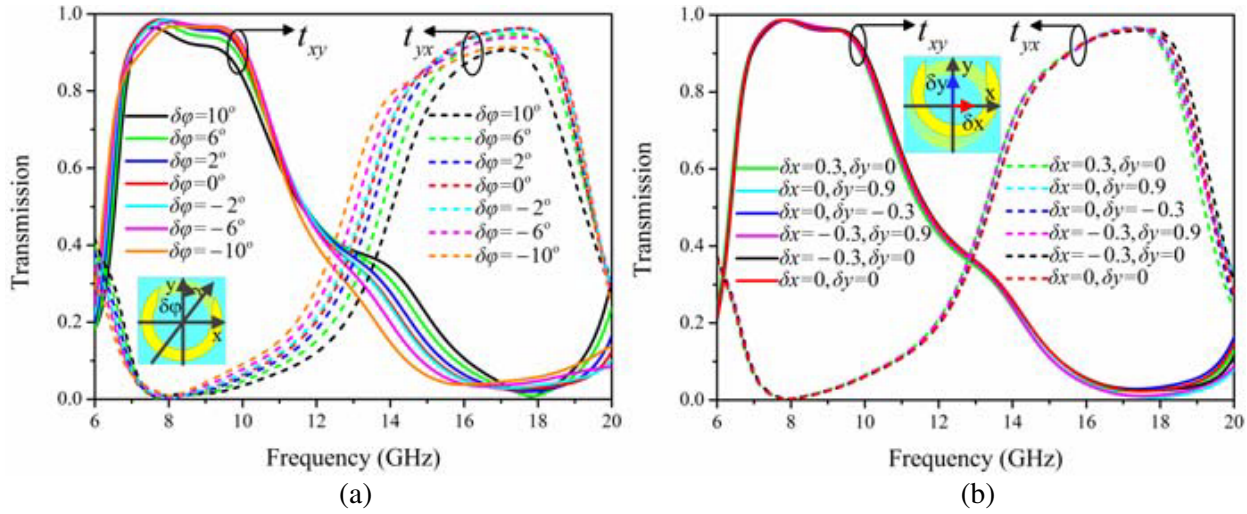

Figure 6. Simulated transmission coefficients as a function of (a) angle misalignment $\delta\varphi$ and transversal misalignment δx and (b) longitudinal misalignment δy.

that the x-polarized incident wave is converted to its cross-polarized wave in the range from 16.46 to 18.47 GHz. These results indicate that the proposed CMM can indeed achieve dual-band polarization conversion for linearly polarized wave, with one band for y-polarized wave and the other for x-polarized wave.

The above results show that the proposed structure has advantages of dual-band and high-efficiency AT effect for linearly polarized wave. However, it is well known that during the layer-by-layer fabrication process, misalignment always occurs and influences the performance of devices [27]. Therefore, the relationship between the alignment errors and AT performance needs to be investigated. Fig. 6(a) gives the simulated cross-polarization transmission coefficients t_{xy} and t_{yx} under differently relative rotation angle $\delta\varphi$. It is shown that the rotation angle misalignments have a very small influence on the dual-band AT effect when the relative rotation angle $|\delta\varphi|$ is increased to 10°. Moreover, the transversal and longitudinal misalignments are also examined here, shown in Fig. 6(b). When the transversal and longitudinal misalignments are $\delta x = 0.3$ and $\delta y = 0.9$, respectively, the transmission curves still almost maintain the same shape as in the perfectly aligned case ($\delta x = \delta y = 0$). These results indicate that the misalignments in the x- and y-directions can be neglected. To verify the effects of these two types

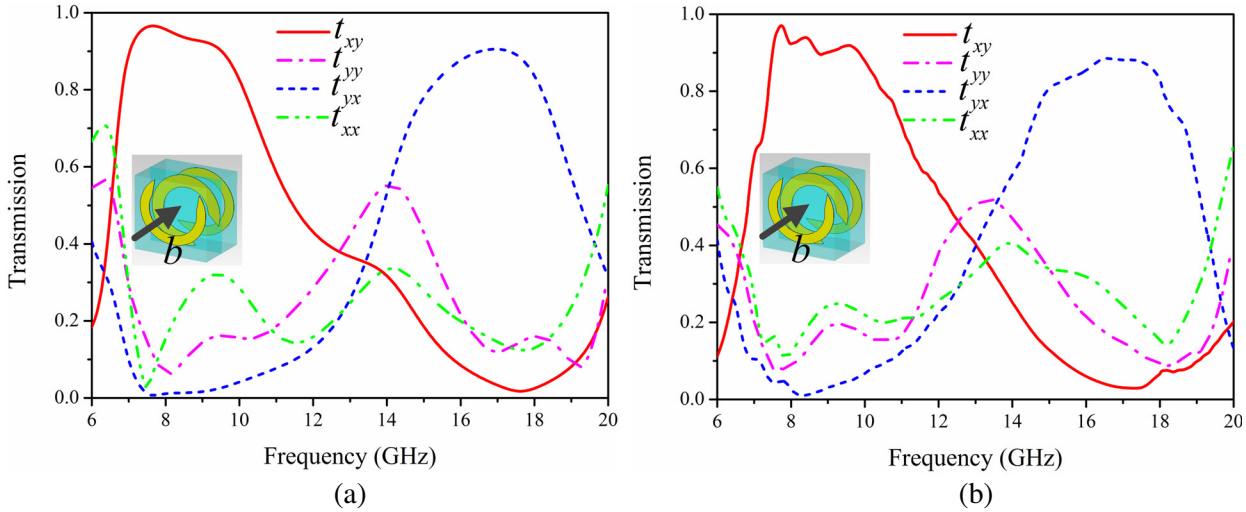

Figure 7. (a) Simulated and (b) measured transmission coefficients for forward propagating wave, when the transversal, longitudinal and angle misalignments δx, δy and $\delta\varphi$ are fixed ($\delta x = 0.3$, $\delta y = 0.9$, $\delta\varphi = -10°$).

of misalignment, we simulated and measured the transmission coefficients for propagation along $-z$ direction in the designed structure as shown in Fig. 7, when $\delta x = 0.3$, $\delta y = 0.9$, and $\delta\varphi = -10°$. The measured transmission coefficients in Fig. 7(b) are similar to the simulated ones in Fig. 7(a). Even though the magnitudes of t_{xy} and t_{yx} are decreased, the obvious AT effect is still sustained at the two bands of X (7.02–9.50 GHz) and Ku (16.60–17.20 GHz). The discrepancy between the simulation and the measurement results were caused by machining errors and measurement errors. In summary, according to the simulated and measured results, the proposed CMM has a good robustness to misalignment that occurs in the layer-by-layer fabrication process, which provides convenience for fabricating in practical applications.

To understand the physical mechanism of the dual-band AT effect, we observed the surface current distributions in each of the SRRs layer (shown in Fig. 8) for EM wave passing through the structure along the forward direction at the resonant frequencies of 7.86 GHz and 17.65 GHz, respectively. At resonances, the incident wave induces longitudinal magnetic dipole and transverse electric dipole excitations inside the proposed CMM, which are associated with current distributions in each of the SRRs layer. Therefore, near-field coupling between neighboring SRRs layer results in an obvious transmitted wave, but the polarization of the transmitted wave has been rotated by nearly 90° [14]. Clearly, as shown in Fig. 8, when a $y(x)$-polarized incident wave passed through the proposed CMM in forward direction, the differently resonant modes of the SRRs corresponding to the top, middle and bottom metallic layers were excited. As Fig. 8(a) shows, at the first resonance frequency of 7.86 GHz for y-polarized wave, both the same and opposite direction currents exist on the top and middle SRRs layers, and the opposite direction currents exist on the middle and bottom SRRs layers, thus causing high cross-coupling between the electric and magnetic fields in the three-layered SRRs structure. Fig. 8(b) shows that at the first resonance frequency of 7.86 GHz for the x-polarized wave, the circular surface current direction on the three SRRs layers are different, which results in the existence of anti-parallel magnetic dipole moments in the three-layered SRRs structure. However, it is clear that when compared with the induced currents for the y-polarized wave, the strength of currents excited by the x-polarized wave are very small. Therefore, the near-field coupling between the neighboring SRRs layers is very weak, and this results in very low cross-polarization transmission. Figs. 8(c) and (d) indicate that, at the second resonance frequency of 17.65 GHz for the $y(x)$-polarized wave, the situation becomes more complex. Figs. 8(c) and (d) show that the current direction for the y-polarized wave is different from the one for the x-polarized incident wave on the top and bottom SRRs layers, and the same current direction only exists on the middle SRRs layer. Additionally, the strength of currents excited by y-polarized wave are very low when compared with the currents excited by x-polarized wave, as shown in Figs. 8(c) and (d). Therefore, the near-field

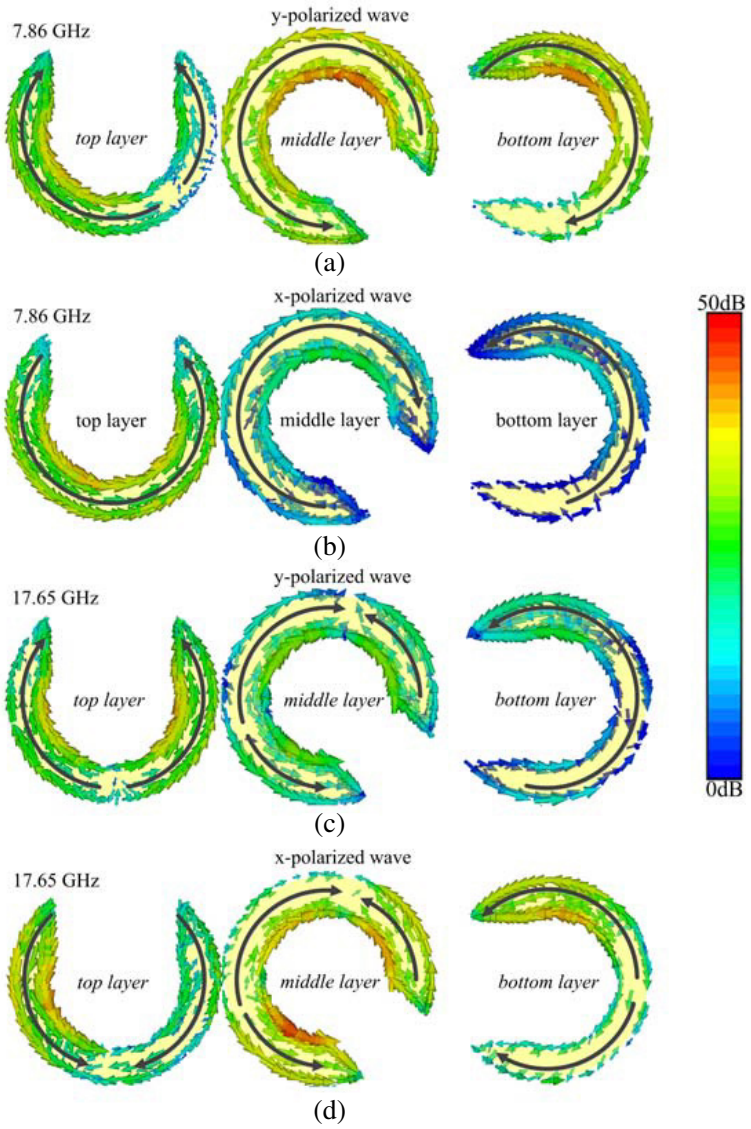

Figure 8. Surface current distributions in the top layer, middle layer and bottom layer at (a), (b) 7.86 GHz and (c), (d) 17.65 GHz.

coupling between the neighboring SRRs layer for the y-polarized incident wave is very weak, and thus results in very low cross-polarization transmission. In Fig. 8(d), the different electric dipole modes of each SRRs layer are excited by the x-polarized incident wave at the resonance frequency of 17.65 GHz. The near-field coupling between the top, middle and bottom SRRs layers then results in obvious cross-polarization transmission. The induced surface current in each of the SRRs layers clearly shows that the excitation of different resonant modes and interlayer near-field coupling among the three-layered SRRs structure are essential for dual-band AT functionality.

5. CONCLUSION

In conclusion, we have numerically and experimentally demonstrated an interesting three-layered CMM that can realize efficient dual-band AT for linearly polarized wave and cross-polarization conversion in the microwave frequency regions. Both the simulated and measured results show that the CMM is nearly transparent to incident linearly polarized wave in two distinct AT bands, where a linearly polarized incident wave can be efficiently converted to its cross-polarized wave and can be transmitted,

while the same linearly polarized incident wave is blocked from traveling in the opposite direction by the CMM. In addition, the simulated and measured results confirm that the proposed CMM has a good robustness to misalignment, which provides convenience for fabricating in practical applications. The physical mechanism of dual-band AT can be explained based on the different resonant modes of the proposed structure. We believe that the proposed CMM has great potential for use as a polarization manipulation device in sensors, antennas and other related applications.

ACKNOWLEDGMENT

The authors are grateful for the support provided by the National Natural Science Foundation (NSF) of China (Grant Nos. 61471292, 61471388, 61331005, 41390454, and 41404095), the National Basic Research Program of China (973 Program) under Grant No. 2015CB654602, and the 111 Project under Grant No. B14040.

REFERENCES

1. Shelby, R. A., D. R. Smith, and S. Schultz, "Experimental verification of a negative index of refraction," *Science*, Vol. 292, No. 5514, 77–79, 2001.
2. Pendry, J. B., D. Schurig, and D. R. Smith, "Controlling electromagnetic fields," *Science*, Vol. 312, No. 5781, 1780–1782, 2006.
3. Fang, N., H. Lee, C. Sun, and X. Zhang, "Sub-diffraction-limited optical imaging with a silver superlens," *Science*, Vol. 308, No. 5721, 534–537, 2005.
4. Ye, Y. and S. He, "90° polarization rotator using a bilayered chiral metamaterial with giant optical activity," *Appl. Phys. Lett.*, Vol. 96, No. 20, 788, 2010.
5. Chen, J. and A. Zhang, "A linear-to-circular polarizer using split ring resonators," *Applied Computational Electromagnetics Society Journal*, Vol. 28, No. 6, 507–512, 2013.
6. Cheng, Y., Y. Nie, Z. Cheng, and R. Z. Gong, "Dual-band circular polarizer and linear polarization transformer based on twisted split-ring structure asymmetric chiral metamaterial," *Progress In Electromagnetics Research*, Vol. 145, 263–272, 2014.
7. Fedotov, V. A., A. S. Schwanecke, N. I. Zheludev, V. V. Khardikov, and S. L. Prosvirnin, "Asymmetric transmission of light and enantiomerically sensitive plasmon resonance in planar chiral nanostructures," *Nano Lett.*, Vol. 7, No. 7, 1996–1999, 2007.
8. Singh, R., E. Plum, C. Menzel, C. Rockstuhl, A. K. Azad, R. A. Cheville, F. Lederer, W. Zhang, and N. I. Zheludev, "Terahertz metamaterial with asymmetric transmission," *Phys. Rev. B*, Vol. 80, No. 15, 153104(5), 2009.
9. Schwanecke, A. S., V. A. Fedotov, V. V. Khardikov, S. L. Prosvirnin, Y. Chen, and N. I. Zheludev, "Nanostructured metal film with asymmetric optical transmission," *Nano Lett.*, Vol. 8, No. 9, 2940–2943, 2008.
10. Plum, E., V. A. Fedotov, and N. I. Zheludev, "Planar metamaterial with transmission and reflection that depend on the direction of incidence," *Appl. Phys. Lett.*, Vol. 94, No. 13, 131901, 2009.
11. Menzel, C., C. Helgert, C. Rockstuhl, E.-B. Kley, A. Tünnermann, T. Pertsch, and F. Lederer, "Asymmetric transmission of linearly polarized light at optical metamaterials," *Phys. Rev. Lett.*, Vol. 104, No. 25, 253902, 2010.
12. Kang, M., J. Chen, H. X. Cui, Y. Li, and H. T. Wang, "Asymmetric transmission for linearly polarized electromagnetic radiation," *Opt. Express*, Vol. 19, No. 9, 8347–8356, 2011.
13. Mutlu, M., A. E. Akosman, A. E. Serebryannikov, and E. Ozbay, "Diodelike asymmetric transmission of linearly polarized waves using magnetoelectric coupling and electromagnetic wave tunneling," *Phys. Rev. Lett.*, Vol. 108, No. 21, 213905, 2012.
14. Huang, C., Y. Feng, J. Zhao, Z. Wang, and T. Jiang, "Asymmetric electromagnetic wave transmission of linear polarization via polarization conversion through chiral metamaterial structures," *Phys. Rev. B*, Vol. 85, No. 19, 195131, 2012.

15. Cheng, Y., Y. Nie, X. Wang, and R. Gong, "An ultrathin transparent metamaterial polarization transformer based on a twist-split-ring resonator," *Appl. Phys. A*, Vol. 111, No. 1, 209–215, 2013.
16. Shi, J. H., Z. Zhu, H. F. Ma, and W. X. Jiang, "Tunable symmetric and asymmetric resonances in an asymmetrical split-ring metamaterial," *Journal of Applied Physics*, Vol. 112, No. 7, 073522, 2012.
17. Dincer, F., C. Sabah, M. Karaaslan, E. Unal, M. Bakir, and U. Erdiven, "Asymmetric transmission of linearly polarized waves and dynamically wave rotation using chiral metamaterial," *Progress In Electromagnetics Research*, Vol. 140, 227–239, 2013.
18. Shi, J., X. Liu, S. Yu, T. Lv, Z. Zhu, H. F. Ma, and T. J. Cui, "Dual-band asymmetric transmission of linear polarization in bilayered chiral metamaterial," *Appl. Phys. Lett.*, Vol. 102, No. 19, 191905, 2013.
19. Shi, J. H., H. F. Ma, C. Y. Guan, Z. P. Wang, and T. J. Cui, "Broadband chirality and asymmetric transmission in ultrathin 90°-twisted Babinet-inverted metasurfaces," *Phys. Rev. B*, Vol. 89, No. 16, 165128, 2014.
20. Pfeiffer, C., C. Zhang, V. Ray, L. J. Guo, and A. Grbic, "High performance bianisotropic metasurfaces: Asymmetric transmission of light," *Phys. Rev. Lett.*, Vol. 113, No. 2, 023902, 2014.
21. Liu, D. Y., M. H. Li, X. M. Zhai, L. F. Yao, and J. F. Dong, "Enhanced asymmetric transmission due to Fabry-Perot-like cavity," *Opt. Express*, Vol. 22, No. 10, 11707–11712, 2014.
22. Song, K., Y. H. Liu, C. R. Luo, and X. P. Zhao, "High-efficiency broadband and multiband cross-polarization conversion using chiral metamaterial," *J. Phys. D: Appl. Phys*, Vol. 47, No. 50, 505104, 2014.
23. Liu, D. J., Z. Y. Xiao, and Z. H. Wang, "Multi-band asymmetric transmission and 90° polarization rotator based on bi-Layered metasurface with F-shaped structure," *Plasmonics*, 2016, DOI: 10.1007/s11468-016-0284-4.
24. Menzel, C., C. Rockstuhl, and F. Lederer, "An advanced Jones calculus for the classification of periodic metamaterials," *Phys. Rev. A*, Vol. 82, No. 5, 053811, 2010.
25. Mutlu, M. and E. Ozbay, "A transparent 90° polarization rotator by combining chirality and electromagnetic wave tunneling," *Appl. Phys. Lett.*, Vol. 100, No. 5, 051909, 2012.
26. Born, M., E. Wolf, and A. B. Bhatia, "Principles of optics: electromagnetic theory of propagation, interference and diffraction of light," Cambridge University, 1999.
27. Ji, R., S. W. Wang, X. Liu, and W. Lu, "Giant and broadband circular asymmetric transmission based on two cascading polarization conversion cavities," *Nanoscale*, Vol. 8, No. 15, 8189–8194, 2016.